13th ewtec 2019 Proceedings of the 13th European Wave and Tidal Energy Conference 1-6 Sept 2019, Naples, Italy

Excitation force estimation for wave energy systems using a moment-domain representation

Jake Cunningham, Nicolás Faedo, and John V. Ringwood

***Abstract*—To maximise the energy converted from a Wave Energy Converter (WEC), a real-time control law is required, which, due to its non-causal nature, necessitates the knowledge of the wave excitation force in future time. This future excitation force time series is usually obtained using forecasting strategies, which are essentially based on present and past values of the wave excitation force. Unfortunately, the excitation force is virtually always a non-measurable quantity, which leads to the necessity of a suitable estimation technique. There have been several methods developed for this unknown-input estimation problem, though some drawbacks can be readily identified. One fundamental issue comes from the convolution term accounting for the effect of radiation forces acting on the WEC. The usual approach is to approximate this convolution operation by a suitable parametric representation. However, in general, a more accurate parametric approximation directly implies a higher dimension of the model representing the WEC dynamics. This can potentially constitute a problem for real-time capabilities as it naturally increases the underlying computational complexity. In this paper, a newly developed moment-based estimator is presented, which does not require of an approximation of the radiation force dynamics. The presented moment-based estimator has been compared to an input-unknown Kalman filter, which represents a benchmark method for excitation force estimation within the wave energy community.**

***Index Terms*—Wave energy, input-unknown estimation, excitation force, moment-domain**

I. Introduction

ONE way to reduce the generating cost of electricity from waves is to maximise the energy extracted from Wave Energy Converters (WECs) [1]. In order to maximise the energy extracted, several optimal control strategies have been developed. Most of these control methods are inherently non-causal, in that they require knowledge of future values of the wave excitation force (input) acting on the WEC, (see [2] and [3]). We note that there are a few sub-optimal control methods, which minimise or eliminate the need to know the excitation force [4]. Nevertheless, as discussed in [3], the vast majority of the optimal energy-maximising control strategies require its future knowledge.

There are some proven codes, such as WAMIT [5] and NEMOH [6], to compute the hydrodynamic parameters of WECs. In particular, WAMIT and NEMOH belong to the family of Boundary Element Methods (BEMs) [7]. However, BEMs solve the radiation and diffraction problems in the frequency-domain and can only characterise the steady-state motion of the WEC under analysis. A more comprehensive dynamical model in the time domain for WECs can be performed by considering the well-known Cummins' equation [8]. There is a direct relationship between Cummins' equation and the hydrodynamics of the WEC in the frequency domain data, which is given in [9]. The final time-domain dynamical model is a integro-differental equation, which includes a convolution term accounting for the effect of radiation forces acting on the device. This convolution term greatly increases the computational complexity.

The future excitation force time series (F_{ex}), which is required for most real-time controllers, is usually obtained using forecasting strategies, which are essentially based on present and past values of F_{ex}. Unfortunately, the excitation force is virtually always a non-measurable quantity, which leads to the necessity for estimation. Previous solutions to the excitation force estimation problem include the Kalman filter and extended Kalman filter ([10], [11], [12] and [13]). However, some drawbacks can be identified. One of the primary drawbacks is within the effect of radiation forces acting on the WEC, more specifically the convolution term accounting for these forces. The usual approach is to approximate this convolution term by a suitable parametric structure. However, in general, accurate approximations of the convolution term increases the dimension of the model representing the WEC dynamics. This can potentially constitute a problem for real-time capabilities, as it naturally increases the computational complexity.

This paper proposes a moment-based excitation force estimator. This strategy is based on recent advances in moment-based theory (particularly in the control and identification areas [14], [15], [16] & [17]), and exploits a particular parametrisation of the steady-state response of the WEC, providing a sensible set of

The paper ID is 1418 and was submitted to conference track GPC. This paper is based upon work supported by Science Foundation Ireland under Grant No. 12/RC/2302 for the Marine Renewable Ireland (MaREI) centre. This material is based upon works supported by Science Foundation Ireland under Grant no. 13/IA/1886.

J. Cunningham is with the Centre for Ocean Energy Research lab in Dept. of Electronic Engineering, Maynooth University, Co. Kildare, Ireland. Email: jake.cunningham.2019@mumail.ie

N. Faedo is with the Centre for Ocean Energy Research lab in Dept. of Electronic Engineering, Maynooth University, Co. Kildare, Ireland. Email: nicolas.faedo@mu.ie

J. V. Ringwood is with the Centre for Ocean Energy Research lab in Dept. of Electronic Engineering, Maynooth University, Co. Kildare, Ireland. Email: john.ringwood@mu.ie

mappings to compute the estimation of the excitation forces, which is intrinsically related to the WEC dynamics. An advantage with this method is that, within the moment-domain, there is no requirement to approximate the radiation force convolution term, thus greatly reducing the computational complexity, leading to improved real-time capability. To the best of our knowledge, this is the first application of the moment-based framework to any state or input estimation problem.

A cylindrical buoy has been considered as an example case in this paper. The device is axisymmetric and has a uniform cross-sectional area, so that linear potential theory can reasonably be applied to the device. It has also been assumed that the device only moves in the heave (vertical) direction, for simplicity.

The remainder of this paper is organised as follows. In Section II, moment-based theory is introduced. In Section III, the linear WEC model is recalled, both in the time-domain and the moment-domain. In Section IV, a moment-based approach to the estimation problem is proposed. This includes an algorithm, to outline the steps involved in a concise method. In Section V, the results are obtained from the case study and discussed. Finally, Section VI contains some concluding remarks.

Notation

Standard notation is considered through this study with any exceptions detailed in this section. $\mathbb{R}^+(\mathbb{R}^-)$ denotes the set of non-negative (non-positive) real numbers. $\mathbb{C}^0$ denotes the set of pure-imaginary complex numbers and $\mathbb{C}^-$ denotes the set of complex numbers with a negative real part. The symbol 0 stands for any zero element, with dimension according to the context. The symbol $\mathbb{I}_n$ denotes a size n identity matrix. The spectrum of a matrix $A \in \mathbb{R}^{n\times n}$, i.e. the set of its eigenvalues, is denoted $\lambda(A)$. The symbol $\bigoplus$ denotes the direct sum of n matrices, i.e. $\bigoplus_{i=1}^{n} A_i = \text{diag}(A_1, A_2, ..., A_n)$. The convolution between two functions $f(t)$ and $g(t)$ over a finite interval $[0, t] \subset \mathbb{R}^+$, i.e $\int_0^t f(\tau)g(t-\tau)d\tau$ is denoted $f(t) * g(t)$. If matrix $A \in \mathbb{R}^{n\times m}$ then $A^\dagger \in \mathbb{R}^{m\times n}$ symbolises the Moore-Penrose inverse. $\epsilon_n \in \mathbb{R}^n$ stands for a vector with odd components equal to 1 and null even components. Within an algorithm a semicolon (;) defines a new row in a matrix and a comma (,) defines a new column in a matrix.

II. Moment-Based Theory

This section briefly reviews linear moment-based theory. The reader is referred to [18] for detailed description of these topics. Consider a finite-dimensional, single-input, single-output, continuous-time system described, for $t \geq 0$, by the state-space model

$$\dot{x}(t) = Ax(t) + Bu(t), \quad y(t) = Cx(t), \tag{1}$$

where $x(t) \in \mathbb{R}^n$, $u(t) \in \mathbb{R}$, $A \in \mathbb{R}^{n\times n}$, $B \in \mathbb{R}^n$ and $C^T \in \mathbb{R}^n$. Consider the associated transfer function

$$H(s) = C(s\mathbb{I}_n - A)^{-1}B, \tag{2}$$

and assume that (1) is minimal (i.e. controllable and observable).

Definition 1 [19] The 0-moment of system (1) at $s_i \in \mathbb{C}\backslash\lambda(A)$ is the complex number $\eta_0(s_i) = C(s_i\mathbb{I}_n - A)^{-1}B$. The k-moment of system (1) at $s_i \in \mathbb{C}$ is the complex number

$$\eta_k(s_i) = \frac{(-1)^k}{k!}\left[\frac{d^k}{ds^k}(C(s\mathbb{I}_n - A)^{-1}B)\right]_{s=s_i}, \tag{3}$$

with $k \geq 1$ an integer. In [18], a novel interpretation of moments is given in terms of the steady-state response (provided it exists) of the output of the interconnection between a signal generator and system (1). The result is recalled in the following theorem.

Theorem 1([18]; [20]) Consider system (1) and the signal generator

$$\dot{\xi}(t) = S\xi(t), \quad u(t) = L\xi(t), \tag{4}$$

with $\xi(t) \in \mathbb{R}^\nu$, $S \in \mathbb{R}^{\nu\times\nu}$, $L^T \in \mathbb{R}^\nu$ and $\xi(0) \in \mathbb{R}^\nu$. Assuming that the triple $(L, S, \xi(0))$ is minimal, $\lambda(A) \subset \mathbb{C}^-$, $\lambda(S) \subset \mathbb{C}^0$ and the eigenvalues of S are simple. Let $\Pi \in \mathbb{R}^{n\times\nu}$ be the unique solution to the Sylvester equation

$$A\Pi + BL = \Pi S. \tag{5}$$

Then, there exists a one-to-one relation between the moments $\eta_0(s_1), \eta_0(s_2), ..., \eta_0(s_\nu)$, with $s_i \in \lambda(S)$ for all $i \in \{1, ..., \nu\}$, and the steady-state response $C\Pi\xi$ of the output y of the interconnection of system (1) with the signal generator (4). Note that, from now on, the matrix $C\Pi = Y$ is referred to as the moment-domain equivalent of $y(t)$.

III. WEC Model

As mentioned in Section I, the WEC hydrodynamical model is based on linear potential theory, consider the fluid is to be inviscid and the flow both irrotational and incompressible. Under these assumptions, the dynamic model of the device is given by:

$$m\ddot{x}(t) = -F_r(t) - F_h(t) + F_{ex}(t) + u(t), \tag{6}$$

where m is the mass of the device, x the device excursion, F_h is the hydrostatic restoring force, F_r is the radiation force, F_{ex} is the excitation force and u represents the control input force, which is supplied by means of a Power Take-Off (PTO) system. $F_h(t) = K_H x(t)$, where K_H denotes the hydrostatic stiffness. The radiation force F_r is modelled from linear potential theory and using the well-known Cummins' equation [8], as

$$F_r(t) = A_\infty\ddot{x}(t) + \int_0^{+\infty} k(\tau)\dot{x}(t-\tau)d\tau, \tag{7}$$

where $A_\infty = \lim_{\omega\to+\infty} A(\omega)$, with $A_\infty \geq 0$ represents the added-mass asymptote at infinity frequency. The control input has been parameterised similarly as in [21].

$$u(t) = m_u\ddot{x}(t) + b_u\dot{x}(t) + K_u x(t), \tag{8}$$

where the values of $\{m_u, b_u, K_u\} \subset \mathbb{R}$ can be obtained by several optimal (or suboptimal) control strategies

[2]. Finally, the complete linearised equation of motion of the WEC is

$$\ddot{x}(t) = \frac{-k(t) * \dot{x}(t) - b_u \dot{x}(t) - (K_u + K_H)x(t) + F_{ex}(t)}{m + A_\infty + m_u}. \tag{9}$$

A. Moment-domain formulation

The equations of motion from (9) are now re-written in a more suitable structure following [14]. For the remainder of this paper, the state-space representation is as follows

$$\dot{\varphi}(t) = A\varphi(t) + B\mathfrak{u}(t), \quad y(t) = C\varphi(t), \tag{10}$$

where $\varphi(t) = [x(t) \quad \dot{x}(t)]^T \in \mathbb{R}^n$, with $n = 2$, is the state-vector continuous time model and $y(t) = \dot{x}(t) \in \mathbb{R}$ is the output of the system. The function $\mathfrak{u}(t) \in \mathbb{R}$ is assumed to be the input. The radiation convolution term has been included as a feedback term purely as an algebraic manipulation to develop the state space representation of (9) and the meaningful input is the wave excitation force, $F_{ex}(t)$, i.e.

$$\mathfrak{u}(t) = F_{ex}(t) - k(t) * \dot{x}(t). \tag{11}$$

The PTO force has been parametrised using the state variables via (8), being now included in the state matrix, A, and the input matrix, B. Therefore, the matrices in (10) are

$$\begin{aligned} A &= \begin{bmatrix} 0 & 1 \\ -\frac{K_H + K_u}{m + A_\infty + m_u} & -\frac{b_u}{m + A_\infty + m_u} \end{bmatrix}, \\ B &= \begin{bmatrix} 0 \\ \frac{1}{m + A_\infty + m_u} \end{bmatrix}, C = \begin{bmatrix} 0 & 1 \end{bmatrix}. \end{aligned} \tag{12}$$

Following [14], F_{ex}, in the moment-based framework, is expressed as a signal generator (see (4)), as

$$\dot{\xi}_{ex}(t) = S\xi_{ex}(t), \quad F_{ex}(t) = L_{ex}\xi_{ex}(t), \tag{13}$$

where the dimension of S is the same as in (4), $L_{ex}^T \in \mathbb{R}^\nu$, $\xi_{ex}(t) \in \mathbb{R}^\nu$ and, without loss of generality, the initial condition of the signal generator is chosen as $\xi_{ex}(0) = \epsilon_\nu$. Since the eigenvalues of S are simple and lie is $\mathbb{C}^0$, S can be written in a real block-diagonal form as

$$S = \bigoplus_{p=1}^{q} \begin{bmatrix} 0 & \omega_p \\ -\omega_p & 0 \end{bmatrix}, \tag{14}$$

where $\nu = 2q$, with $q \geq 0$ integer. Note that, with this selection of matrices, the assumption on the minimality of the triple $(L_{ex}, S, \epsilon_\nu)$ holds as long as (L_{ex}, S) is observable.

One usual assumption for the numerical generation of the wave excitation force, in many ocean engineering applications, is that it can be described as the sum of several frequency components [22]. Note that this is indeed the same class of input induced by the signal generator (13)-(14). Based on this selection of matrices, the moments of system (10), driven by the signal generator (13), can be computed by solving a Sylvester equation (5). [14] Considering superposition, the Sylvester equation for the WEC device case can be written as

$$A\Pi + B(L_{ex} - \bar{R}) = \Pi S, \tag{15}$$

where $\Pi \in \mathbb{R}^{n \times \nu}$ and $\bar{R}^T \in \mathbb{R}^\nu$ is the moment-domain equivalent of the state and radiation convolution term respectively. Proof of this statement can be found in [14], and is briefly summarised below for convenience. The moment-domain equivalent of the convolution term is as follows:

$$\bar{R} = V\mathcal{R}, \tag{16}$$

where $\mathcal{R} \in \mathbb{R}^{\nu \times \nu}$ is a diagonal block matrix defined by

$$\mathcal{R} = \bigoplus_{p=1}^{q} \begin{bmatrix} \mathfrak{r}_{\omega_p} & -\mathfrak{m}_{\omega_p} \\ \mathfrak{m}_{\omega_p} & \mathfrak{r}_{\omega_p} \end{bmatrix}, \tag{17}$$

and its entries depend on the added mass $A(\omega)$ and the radiation damping $B(\omega)$ of the device at each specific frequency induced by the eigenvalues of S, as

$$\mathfrak{r}_{\omega_p} = B(\omega_p), \quad \mathfrak{m}_{\omega_p} = -\omega_p[A(\omega_p) - A_\infty]. \tag{18}$$

$A(\omega)$ and $B(\omega)$ are obtained by using hydrodynamic solvers, such as WAMIT or NEMOH. Note that the relationship of these coefficients with time-domain analysis can be found in [9].

IV. Estimation

This section presents an estimator in the moment-domain for F_{ex}, which uses the measurements of the position of the device to compute an estimate of such a signal. This study deals with the dynamical system model as in (10), (11) and (12). Following (13), the estimated excitation force is defined as,

$$\hat{F}_{ex}(t) = \hat{L}_{ex}\xi_{ex}(t), \tag{19}$$

where the dimension of $\xi_{ex}(t)$ is as in (13) and $\hat{L}_{ex}^T \in \mathbb{R}^\nu$. The assumption on the minimality of the triple $(\hat{L}_{ex}, S, \epsilon_\nu)$ holds as long as the pair $(\hat{L}_{ex}, S)$ is observable. For the estimation problem, each of the ω_p represents an element of the finite set of frequencies chosen to map out the spectrum of the sea state. Using (13), $\xi_{ex}(t)$, can be computed as follows:

$$\xi_{ex}(t) = \exp[St]\epsilon_\nu = \begin{bmatrix} \cos(\omega_1 t) \\ -\sin(\omega_1 t) \\ \vdots \\ \cos(\omega_q t) \\ -\sin(\omega_q t) \end{bmatrix}. \tag{20}$$

The steady-state of the WEC is related to the moment representation by the solution of the signal generator (13),

$$\varphi_{ss}(t) = \Pi\xi_{ex}(t). \tag{21}$$

The state-vector is comprised of the position and the velocity of the system, and the output is the velocity. Note that Π can be partitioned similarly to φ:

$$\Pi = \begin{bmatrix} X \\ V \end{bmatrix}, \tag{22}$$

where $X^T \in \mathbb{R}^\nu$ and $V^T \in \mathbb{R}^\nu$ are the moment-domain equivalent of position and velocity, respectively. From [23] the moment-domain equivalent of $\dot{x}(t)$, denoted as V, can be computed in terms of X, i.e.,

$$V = XS. \tag{23}$$

Using (23), (22) can be re-written as:

$$\Pi = \begin{bmatrix} X \\ XS \end{bmatrix}, \tag{24}$$

where $(XS)^T \in \mathbb{R}^\nu$. Using (21) and (24) the steady-state position is given by $x_{ss}(t) = X\xi_{ex}(t)$.

B. Estimation within time window

One possible approach to approximate the moment-domain equivalent of the position, where $\hat{X}$ is the approximate of X, is to define a set of specified time instants, i.e. $\mathcal{T} = \{t_1, \ldots, t_n\} \subset \mathbb{R}^+$, where $t_{i+1} - t_i = \tau$. At these time instants the position is measured and the signal generator is evaluated. Then by selecting a time window, of size $dt_i = t_{i+m} - t_i$, within the specified time instances, the matrices below can be built:

$$\begin{aligned} \Xi_i &= [\xi_{ex}(t_i) \ldots \xi_{ex}(t_{m+i})], \\ \Lambda_i &= [x(t_i) \ldots x(t_{m+i})], \end{aligned} \tag{25}$$

where $\Xi_i \in \mathbb{R}^{\nu \times m}$ and $\Lambda_i^T \in \mathbb{R}^m$. Building (25) in such a way enables the approximated moment-domain equivalent of position to be expressed as,

$$\hat{X}_i = \Lambda_i \Xi_i^\dagger, \tag{26}$$

where $\hat{X}_i^T \in \mathbb{R}^\nu$ and $\Xi_i^\dagger \in \mathbb{R}^{m \times \nu}$. Using (23) and (26), the moment-domain equivalent of the state for time window dt_i, i.e. $\hat{\Pi}_i$, can be readily approximated. Consequently, using $\hat{\Pi}_i$, $\hat{L}_{ex_i}$ can be calculated, for dt_i, by rearranging (18) as

$$\hat{L}_{ex_i} = -(BB^T)^{-1}B^T(A\hat{\Pi}_i - \hat{\Pi}_i S + B\hat{\bar{R}}_i), \tag{27}$$

where $(BB^T)^{-1}$ always exists since B is full-column rank [24] and $\hat{\bar{R}}_i$ is the approximation of the moment-domain equivalent of the radiation convolution term, $\hat{\bar{R}}_i = \hat{X}_i S\mathcal{R}$. Using (19) and (27), it is straightforward to compute the estimate of the excitation force for this time window, at time t_{m+i}, as $\hat{F}_{ex}(t_{m+i}) = \hat{L}_{ex_i}\xi(t_{m+i})$. However, this is only for one time window, therefore, after sliding the time window by one specified time instant, $i \to i+1$, everything from the beginning of this subsection can be repeated to compute $\hat{F}_{ex}$ for the next time window.

Algorithm 1 Moment-based estimation

```
procedure Moment estimation(T,A,B,S,R,ξ_ex,x)
T = {t_1, ..., t_n}
n = length(T).
m = length of time window
for i = 1; i ≤ n − m; i++ do
    for j = i; j ≤ i + m; j++ do
        Λ_i = x(t_j).
        Ξ_i = ξ(t_j).
    end
    X̂_i = Λ_i Ξ_i^†.
    V̂_i = X̂_i S.
    Π̂_i = [X̂_i; V̂_i].
    L̂_ex_i = −(BB^T)^{-1} B^T (AΠ̂_i − Π̂_i S + BV̂_i R).
    F̂_ex(t_{i+m}) = L̂_ex_i ξ(t_{i+m}).
end
```

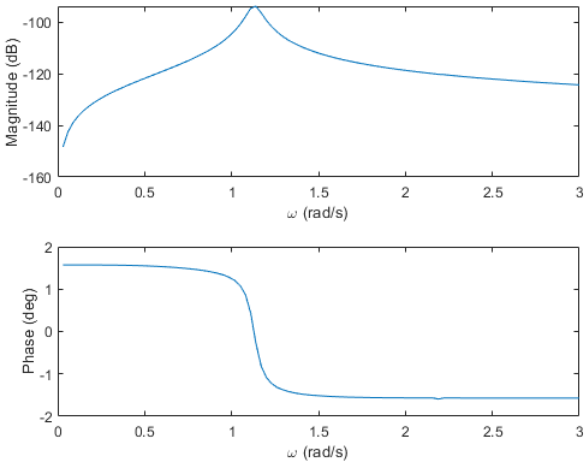

Fig. 1. Bode diagram of the force-to-velocity frequency response, $H(j\omega)$, for the device computed with WAMIT

C. Algorithm layout

The moment estimator algorithm shown in Algorithm 1 requires 7 inputs. $\mathcal{T}$ is the set of time instants, $\mathcal{T} = \{t_1, \ldots, t_n\} \subset \mathbb{R}^+$, A and B can be found in (12), S can be found in (14), $\mathcal{R}$ in (17), ξ_{ex} in (20) and $x(t_i) \in \mathbb{R}$, represents the measurement of position at time t_i. Defining a time window as $\mathcal{T}_i = \{t_i, \ldots, t_{i+m}\} \subset \mathcal{T}$, each cycle of the first for loop represents a time window and, once F_{ex} has been computed for the loop, the window is shifted and the steps repeated.

V. Results & Discussion

As mentioned in the Section I, a cylindrical heaving buoy is the device selected to test the moment estimator. The device parameters are shown in Table I:

TABLE I
PARAMETERS OF WEC MODEL

Parameter	Symbol	Value
Radius	r	5.0 m
Length	L	10.0 m
Draft	h	5.0 m
Mass	m	4×10^5 kg

Applying the Fourier transform to (9) and considering the velocity as the measured output, the following is obtained

$$\dot{\hat{x}}(j\omega) = \bar{F}_{ex}(j\omega)H(j\omega), \tag{28}$$

where $H(j\omega)$ denotes the force-to-velocity response. Note that the expression force-to-velocity is used here to denote the frequency response of the WEC considering the excitation force as the input to the system and velocity as the output, i.e.

$$H(j\omega) = \frac{1}{b_u + B(\omega) + j\omega[A(\omega) + m + m_u] + \frac{K_H + K_u}{j\omega}}. \tag{29}$$

Without any loss of generality, it is assumed in the following case study that $m_u = b_u = s_u = 0$, i.e. there is no presence of a control input. From Fig. 1,

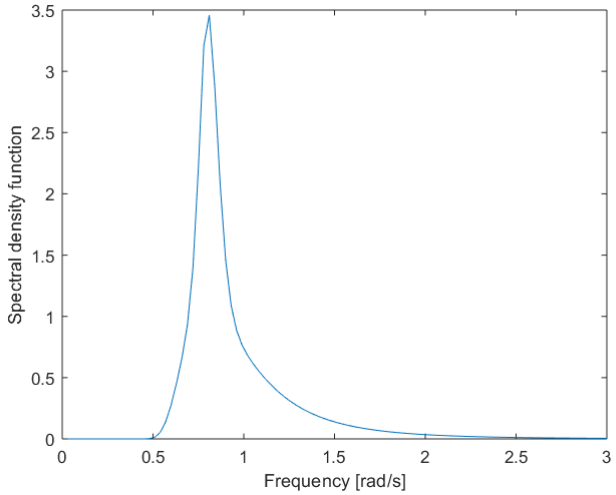

Fig. 2. JONSWAP spectrum considered for the results

TABLE II
TO DETERMINE THE TIME WINDOW SIZE

Size of time window	Accuracy (%)	Computation time (μs)
q	94.85	13.61
2q	96.79	30.2
3q	97.05	37.15

i.e. the Bode diagram of the force-to-velocity frequency response of the device obtained through WAMIT, the resonant frequency of the device can be seen to be ≈ 1.2 rad/s.

For the numerical values in the results, a JONSWAP spectrum is used to reproduce the wave conditions [25], i.e.

$$E(f) = \alpha g^2 (2\pi)^{-4} f^{-5} \exp\left[-\frac{5}{4}\left(\frac{f}{f_p}\right)^{-4}\right] \gamma^{\exp\left[-\frac{f-f_p}{2\sigma^2 f_p^2}\right]}, \tag{30}$$

where g is the acceleration due to gravity, α is the spectral energy parameter, where $\alpha = 5.061 \frac{H_s^2}{T_p^4}(1 - 0.287\ln(\gamma))$, the peak enhancement factor $\gamma = 3.3$, σ is the spectral width parameter, where $\sigma = 0.07(f \leq f_p)$ and $\sigma = 0.09(f > f_p)$ for a realistic sea-state (referenced in [26] and [27] for Pico island). The present results were obtained using a significant wave height of $H_s = 1.5$m and peak period of $T_p = 8$s (please see Fig. 2). First the window size, dt, is investigated. The sampling time is $t_{i+1} - t_i = \tau = 0.05$s.

D. Time Window Size

Two crucial aspects of an estimator are the accuracy of the estimate and the computation time it requires. To remain consistent, the same number of frequencies are used in the comparison of the window size. Three different size windows are investigated, $q\tau, 2q\tau$ and $3q\tau$, where q is the number of frequencies, and $\tau = 0.05$s is the sampling time. 5 frequencies were chosen for the signal generator, $\omega_p \in \{0.4, 0.8, 1.2, 1.6, 2\}$. The

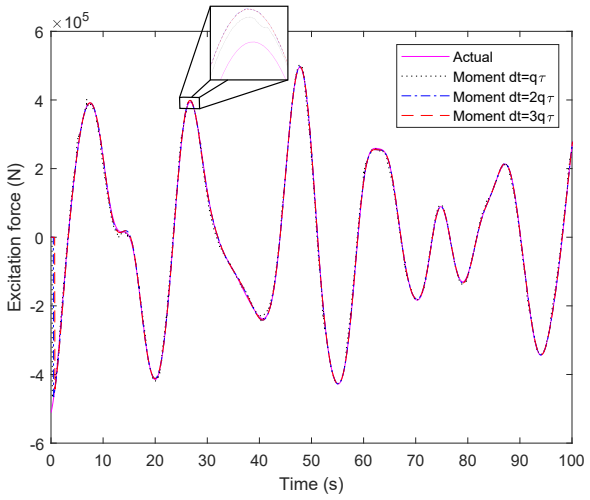

Fig. 3. Actual excitation force and estimated using the Moment-based estimator with windows of size $q\tau$, $2q\tau$ and $3q\tau$, where q is the number of frequencies and τ is the sampling time and equal to 0.05s. Five frequencies used $\omega_p \in \{0.4, 0.8, 1.2, 1.6, 2\}$.

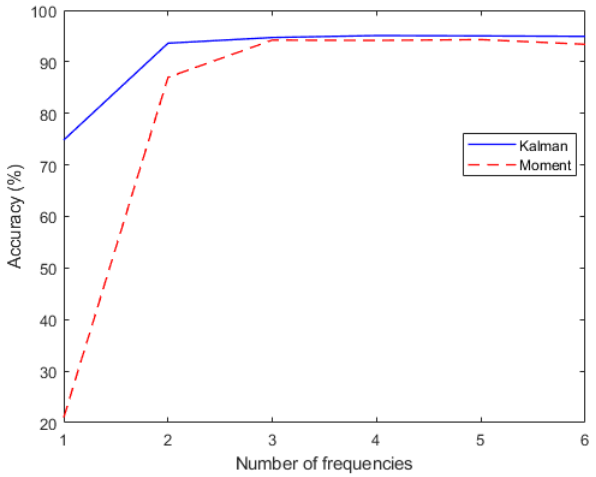

Fig. 4. The accuracy of the estimator for different numbers of frequencies.

accuracy is obtained using the Normalised Root Mean Square Accuracy (NRMSA) formula:

$$\text{NRMSA} = \left(1 - \frac{\sqrt{\sum_{k=1}^{N}(f_k - \hat{f}_k)^2}}{\sqrt{\sum_{k=1}^{N}(f_k)^2}}\right) 100, \tag{31}$$

where N is the number of estimated values. From Table II can be seen that the larger time windows are more accurate. However, the computation time is substantially longer. Therefore, for the purpose of this paper, the size of the time window will be $q\tau$ for the rest of the paper.

As a baseline, the moment-based estimator is compared to the Kalman filter with harmonic oscillator that can be found in [10], [11] and [12]. In these papers, the excitaition force has been modelled the same as (13). However, a state space representation has been interchanged for the radiation convolution term, for the Kalman filter, which can be found in [14]. Three

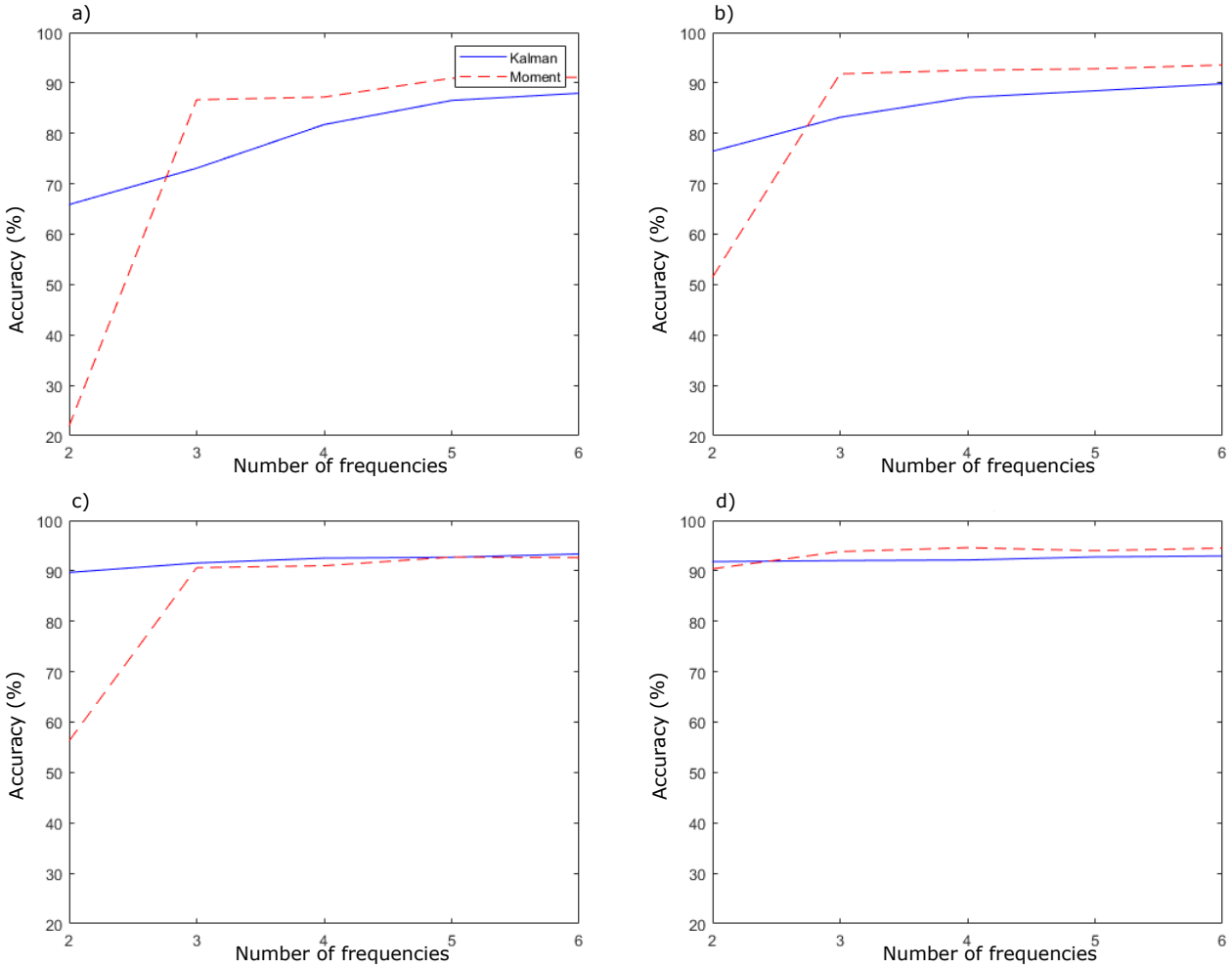

Fig. 5. The accuracy of the estimator. a) completely random frequencies, b) random frequencies and the resonant frequency of the device, c)random frequencies and the peak of the JONSWAP spectrum used and d) random frequencies with the resonant frequency of the device and the peak of the spectrum.

different aspects of the estimators have been compared, the accuracy, the sensitivity to frequency selection and the computation time.

E. Accuracy

When choosing the finite set of frequencies for the signal generator, key frequencies should be considered. The resonant frequency of the device, 1.2 rad/s, and the peak of the JONSWAP spectrum, 0.8 rad/s, are examples of such frequencies. With this information, the frequencies chosen start at $\omega_0 = 0.4$ rad/s, and the peak of the JONSWAP spectrum used, $2\omega_0 = 0.8$ rad/s, and the resonant frequency of the device, $3\omega_0 = 1.2$ rad/s, are then the second and third harmonic receptively. Using (31) as a metric, the accuracy of the estimation has been investigated.

As shown in Fig. 4, the NRMSA increases with the number of frequencies used, as expected. However, it can be seen that the moment-based estimator performs worse than the Kalman filter when only one or two frequencies are used in the estimation. When three or more frequencies are chosen the estimation accuracy stabilises at 94.6% for the Kalman filter and 94.21%. Any increase in the number of frequencies increases the computational complexity, which is explored in Section V.G.

F. Sensitivity to frequency selection

This section investigates the performance of the estimator and its sensitivity to frequency selection. Four different frequency selection methods are considered to test the sensitivity. Method one assumes there is no knowledge of the device or the sea state where the device is situated, the frequencies are chosen randomly where $\omega_p \in [0, 3]$. The next two methods assumes knowledge of either the peak of the spectrum or the resonant frequency of the device followed by randomly generated frequencies. The fourth method assumes knowledge of both of these frequencies. The remainder of the frequencies are then randomly generated. Similar to the previous section, (31) was used as a metric for the accuracy of the estimation.

However, running only one simulation for one set of randomly generated frequencies would lead to results which may not be statistically significant. Therefore, 1000 simulations were run, with different randomly generated frequencies each time. To determine how many simulations must be carried out to obtain a

statistically significant NRMSA value, the central limit theorem was assumed. Using the variance of the simulations and the central limit theorem, to obtain a 95% confidence interval it is found that 410 simulation are necessary to achieve this with a half-width of 0.25% of the mean [12]. This means that, for a given average NRMSA estimate obtained from 410 simulations, there is a 95% probability that the actual average NRMSA lies within $\pm 0.25\%$ of the estimated average NRMSA

From Fig. 5, the importance of the choice of key frequencies is clear. However, the moment-based estimator can still achieve accurate estimation provided at least three frequencies are included in the signal generator. It is possible to choose the frequencies from a forecasted sea spectrum given by meteorological agencies, and adapt them as the sea state changes. However, it is worth to highlight the moment-based estimator is more robust with the frequency selection.

G. Computation time

As mentioned in the introduction, one of the motivators for the development of this new estimator is the potential to reduce the computational complexity to improve real-time capability. The potential comes, in particular, from the moment-based representation of the radiation convolution term. The computation time has been examined from two frequencies to six frequencies. Similar to Section V, 1000 simulations were run and the computation time for one step of the estimation was computed, from these simulations the variance was calculated to obtain the amount of simulations needed to run using the central limit theorem. It was found that to achieve a 95% confidence interval 30 simulation are needed to achieve this with a half-width of 0.25% of the mean. The results are contained in Table III.

TABLE III
COMPUTATION TIME

Number of Frequencies	**Moment (μs)**	**Kalman (μs)**	**% of Improvement**
2	9.36	10.24	$+8.59$
3	10.57	11.27	$+6.21$
4	12.17	14.14	$+13.93$
5	13.61	16.19	$+15.94$
6	16.44	18.21	$+9.72$

It can be seen that the computation time for each step of the estimation increases with the number of frequencies, which was expected as increasing the number of frequencies increases the dimension of the moment representation of the state. It can also be seen that for each computation step the moment estimator is effectively quicker by at least 6.21%.

VI. CONCLUSION

In this paper, a new excitation force estimator has been built using linear based theories in the moment-domain. Accurate estimates are needed for forecasting to deal with the non-causal nature of the majority of controllers to maximise the energy extracted. This is mainly motivated by recent advances in moment-based theory and the ability it contains for dealing with the radiation convolution term.

The moment-based estimator only requires the position measurements to obtain an estimate. It can be seen that, provided at least 3 frequencies are chosen, the moment-based estimator provides a slightly worse estimate than the Kalman filter when the frequencies were chosen to be harmonics of 0.4 rad/s. However, when the frequencies were chosen randomly, with at least three frequencies, the moment-based estimator proved to be similar or better. Therefore, the moment-based estimator is more robust for the frequency selection, provided at least three are chosen. From Section V. F, it is clear to see the importance of key frequencies, such as the resonant frequency of the device and the peak of the spectrum, within the estimation.

Further work will investigate the size of the time-window used to compute the estimate of the excitation force, and different sampling times to further improve the computational time. Additionally, a correction term is to be included in the computation of the Sylvester equation, aiming to provide robustness to a certain class of modelling errors.

REFERENCES

[1] A. Clément, P. McCullen, A. Falcão, A. Fiorentino, F. Gardner, K. Hammarlund, G. Lemonis, T. Lewis, K. Nielsen, S. Petroncini, M. T. Pontes, P. Schild, B. O. Sjöström, H. C. Sørensen & T. Thorpe, "Wave energy in Europe : current status and perspectives," Renewable Sustain. Energy Rev., vol. 6, pp. 405–431, 2002.

[2] J.V. Ringwood, G. Bacelli, F. Fusco, "Energy-maximizing control of wave-energy converters: the development of control system technology to optimize their operation". IEEE Control Systems, vol 34, no. 5, pp. 30–55, Oct. 2014.

[3] N. Faedo, S. Olaya, J. V. Ringwood, "Optimal control, MPC and MPClike algorithms for wave energy systems: An overview", IFAC Journal of Systems and Control, pp. 37-56, Sept., 30, 2017.

[4] A. Falcão, "Phase control through load control of oscillating-body wave energy converters with hydraulic PTO system," Ocean Engineering, vol. 35, no. 3-4, pp. 358–366, 2008.

[5] M. WAMIT Inc., *WAMIT v7.0 manual*, 2013

[6] *NEMOH software*. [Online]. Available: https://lheea.ec-nantes.fr/doku.php/emo/nemoh/start

[7] M. Penalba, T. Kelly, & J.V. Ringwood. "Using NEMOH for modelling wave energy converters: A comparative study with WAMIT", *In Proceedings of the 12th European Wave and Tidal Energy Conference (EWTEC2017)*, p. 631, September 2017.

[8] W. Cummins. "The impulse response function and ship motions" Technical report, DTIC Document, 1962.

[9] T. Ogilvie, "Recent progress toward the understanding and prediction of ship motions" in *Proc. of the 5th Symposium on Navan Hydrodynamics, Bergen, Norway*, ser. ONR, vol. ACR-112, pp. 3-79, September 1964.

[10] M. Garcia-Abril, F. Paparella, and J. V. Ringwood. "Excitation force estimation and forecasting for wave energy applications" *IFAC-PapersOnLine*, vol. 50, no. 1, pp. 14692-14697, 2017.

[11] B. A. Ling, and B. A. Batten, "Real time estimation and prediction of wave excitation forces and a heaving body" *in SME. International Conference on Offshore Mechanics and Arctic Engineering: Ocean Renewable Energy*,Vol. 9, May 2015.

[12] Y. Peña-Sanchez, M. Garcia-Abril, F. Paparella and J. V. Ringwood, "Estimation and Forecasting of Excitation Force for Arrays of Wave Energy Devices," in IEEE Transactions on Sustainable Energy, vol. 9, no. 4, pp. 1672-1680, Oct. 2018.

[13] S. Mhatre, "Application of a linear optimal estimator on a wave energy converter using bang-singular-bang control," Master's thesis, Michigan Technological University, Michigan, USA, 2017.

[14] N. Faedo, Y. Peña-Sanchez, & J. V. Ringwood. "Finite-order hydrodynamic model determination for wave energy applications using moment-matching". *Ocean Engineering*, vol. 163, pp. 251–263, 2018.
[15] N. Faedo, G. Scarciotti, A. Astolfi, & J. V. Ringwood. Energy-maximising control of wave energy converters using a moment-domain representation. *Control Engineering Practice*, vol. 81, pp. 85–96, 2018.
[16] N. Faedo, Y. Peña-Sanchez, and J. V. Ringwood. "Moment-Matching-Based Identification of Wave Energy Converters: the ISWEC Device". IFAC-PapersOnLine, vol. 51, no. 29, pp. 189–194, 2018.
[17] N. Faedo, and J. V. Ringwood. "Moment-Based Constrained Optimal Control of Wave Energy Converters: Flap-Type Device". IFAC-PapersOnLine, vol. 51, no. 29, pp. 50–55, 2018.
[18] A. Astolfi, "Model reduction by moment-matching for linear and nonlinear systems" in *IEEE Transactions on Automatic Control*, vol. 55, no. 10, pp. 2321-2336, 2010
[19] A.C. Antoulas, "Approximation of large-scale dynamical systems", volume 6, SIAM, 2005.
[20] G. Scarciotti & A. Astolfi. "Data-driven model reduction by moment matching for linear and nonlinear systems". Automatica, vol. 79, pp. 340–351, 2017.
[21] J. V. Ringwood, M. Alexis, N. Faedo, F. Fusco, "On the sensitivity and robustness of wave energy control systems", IFAC-PapersOnLine, Vol. 51, no. 29, pp. 62-67, 2018.
[22] A. Mérigaud, & J. V. Ringwood, "Free-surface time-series generation for wave energy applications". IEEE Journal of Oceanic Engineering, vol. 43, no. 1, pp. 19-35, Jan. 2018.
[23] G. Scarciotti & A. Astolfi, "Moment-based discontinuous phasor transform and its application to the steady-state analysis of inverters and wireless power transfer systems". IEEE Trans. Power Electron. vol. 31, no. 12, pp. 8448–8460, 2016.
[24] G.H. Golub & C.F. Van Loan, "Matrix Computations (3rd Ed.)". Johns Hopkins University Press, Baltimore, MD, USA, 1996.
[25] K. Hasselmann, T.P. Barnett, E. Bouws, H. Carlson, D.E. Cartwright, K. Enke, J.A. Ewing, H. Gienapp, D.E. Hasselmann, P. Kruseman, A. Meerburg, P. Muller, D.J. Olbers, K. Richter, W. Sell, & H. Walden. "Measurements of Wind-Wave Growth and Swell Decay during the Joint North Sea Wave Project (JONSWAP)". Ergnzungsheft zur Deutschen Hydrographischen Zeitschrift Reihe, p.95, 1973.
[26] K. Monk, D. Conley, M. Lopes, & Q. Zou, "Pneumatic Power Regulation by Wave Forecasting and Real-Time Relief Valve Control for an OWC", 10th European Wave and Tidal Energy Conference, 2013
[27] F. Paparella, K. Monk, V. Winands, M.F.P. Lopes, D. Conley, & J. V. Ringwood,. "Up-wave and autoregressive methods for short-term wave forecasting for an oscillating water column". IEEE Transactions on Sustainable Energy, vol. 6, no. 1, pp. 171–178, 2015.